Abnormal flow of α particles in heavy-ion collisions at intermediate energies

G. Qu (曲国峰),[1] Y. Huang (黄宇),[1] D. Peng (彭丹),[2] Z. Xu (徐子虚),[1] W. Lin (林炜平),[1] H. Zheng (郑华),[3] G. Tian (田国玉),[4] R. Han (韩瑞),[4] C. Ma (马春旺),[2] M. Huang (黄美容),[6] P. Ren (任培培),[1] J. Han (韩纪锋;),[1] Z. Yang (杨振雷),[7] X. Liu (刘星泉),[1,*] and R. Wada[2,5]

[1]*Key Laboratory of Radiation Physics and Technology of the Ministry of Education, Institute of Nuclear Science and Technology, Sichuan University, Chengdu 610064,China*

[2]*School of Physics, Henan Normal University, Xinxiang 453007, China*

[3]*School of Physics and Information Technology, Shaanxi Normal University, Xi'an 710119, China*

[4]*Institute of Modern Physics, Chinese Academy of Sciences, Lanzhou 730000, China*

[5]*Cyclotron Institute, Texas A&M University, College Station, Texas 77843, USA*

[6]*College of Physics and Electronics information, Inner Mongolia University for Nationalities, Tongliao 028000, China*

[7]*Science and Technology on Reactor System Design Technology Laboratory, Nuclear Power Institute of China, Chengdu 610213, China*

(Received 3 December 2020; accepted 29 March 2021; published 12 April 2021)

The experimentally observed abnormal α flow behavior from heavy-ion collisions at intermediate energies is investigated using the events of $^{40}Ca + ^{40}Ca$ at 35 MeV/nucleon simulated with an improved antisymmetrized molecular dynamics model with specific consideration of the Fermi motion in the nucleon-nucleon collision process. Its possible origins in the processes from the fragment formation to the experimental flow extraction, i.e., dynamical process, sequential decay, experimental detection, and data analysis, are closely examined. It is found that the observed abnormal α flow behavior originates from the reconstruction of reaction planes in the flow extraction. How the abnormal α flow behavior is generated from the reaction plane reconstruction procedure is discussed.

DOI: 10.1103/PhysRevC.103.044607

I. INTRODUCTION

Transverse flow, which is a typical anisotropic collective motion of nuclear matter produced in heavy-ion collisions, has been studied both experimentally and theoretically for several decades, as it carries the crucial information on hot and dense nuclear matter, such as the behavior of nuclear equation of state (EOS) at high densities governing the compression, the internal structure and many other basic properties in supernovae and neutron stars [1–3]. Experimental studies have been performed by varying experimental parameters, such as the beam energy, the combination of projectile and target, the degree of reaction violence, etc., to gain insights into the dependence of transverse flow on these experimental parameters [4–14]. Meanwhile, theoretical studies have focused on using microscopic transport theory in attempt to establish the relation between the measured flow and key inputs in physics and understand the generation mechanism of transverse flow in detail [15–23]. It has been well addressed that the mean field, the symmetry energy, the Coulomb force, and the nucleon-nucleon (NN) collision cross sections are closely related to the flow generation at early stages. That is, at low incident energies (several tens MeV/nucleon), a negative flow pattern is generated, due to the dominant attractive mean-field interaction between projectile and target. As the incident energy increases, the flow tends to be less negative, due to the increasing dominance of the in-medium NN collisions with incident energy. At a certain incident energy (referred as balance energy), the flow becomes zero, and then the flow increases positively as the incident energy increases continually up to hundreds MeV/nucleon. For detailed investigation on the mechanism of flow generation via the comparison between experimental and theoretical results, ambiguities in experiment and theory, such as the complex conditions in experiments and data analyses [10,11,24–26], and the different modeling assumptions resulting in different dynamics in theoretical calculations [27–29], have to be taken into account carefully.

In heavy-ion collisions at intermediate energies, both light charged particles with $Z \leqslant 2$ (LCPs) and intermediate mass fragments with $Z > 2$ (IMFs) are copiously produced. However, only LCPs were often focused on in early studies of transverse flow [30,31]. In 1996, Huang *et al.* first experimentally measured the flow from LCPs and IMFs, and observed a significant dependence of transverse flow on fragment mass in $^{84}Kr + ^{197}Au$ collisions at an incident energy above the balance energy, 200 MeV/nucleon [4]. The obtained flow increases smoothly with mass at the mass range of $1 \leqslant A \leqslant 12$, with the exception of $A = 4$ particles (mainly α particles), and the abnormal $A = 4$ flow becomes even more significant by comparing the experimental results with those from thermodynamic model calculations in the overall mass range [4] (see Fig. 1). Later, D. Cussol *et al.* measured the flow for LCPs and IMFs up to $Z > 10$ from collisions of Ar+Ni and Ni+Ni at incident energies from 30 to 100 MeV/nucleon using the

*liuxingquan@scu.edu.cn

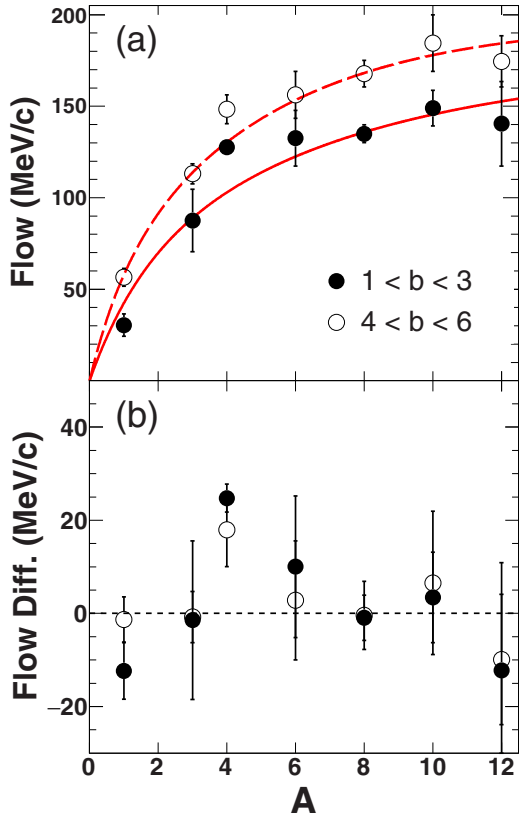

FIG. 1. (a) Mass dependence of transverse flow from the ^{84}Kr + ^{197}Au collisions at 200 MeV/nucleon within the two impact parameter gates, i.e., $1 < b < 3$ fm (filled circles) and $4 < b < 6$ fm (open circles), taken from Ref. [4]. Solid and dashed lines show the corresponding thermodynamic calculations to reproduce the flow values in the overall mass range. (b) The difference between the experimentally extracted flows and those from thermodynamic model calculations at given masses.

INDRA multidetector at GANIL [26]. Their results show that the significant flow enhancement for the $Z = 2$ particles, dominated by α particles, also exists at low incident energies below the balance energy. Recently, we studied the global dependence on mass for the transverse flow in the ^{40}Ca + ^{40}Ca collisions at 35 MeV/nucleon [32]. We also noticed a similar abnormal α flow enhancement, further confirming the abnormal flow behavior for α particles in heavy-ion collisions at intermediate energies. However, it was not able to be clearly addressed in that work due to the mutual interference among the effects from the dynamics and decay processes, the imperfect experimental fragment detection and the data analyses etc, although the experimental flow trend with mass were reproduced by the constrained molecular dynamics (CoMD) model calculations [33,34], in general [32]. Up to now, the dynamical mechanism of the abnormal flow for α particles in heavy-ion collisions at intermediate energies remains puzzling.

A series of unique phenomena related to α particles have been observed experimentally in nuclear collisions, i.e., the similar production cross sections of α particles as compared to nucleons in heavy-ion collisions [35], the observation of α cluster states in $A \leqslant 40$ nuclei [36,37], etc. One of the most effective tools to investigate these α-related phenomena is the antisymmetrized molecular dynamics (AMD) of Ono *et al.* [38,39], due to its capability to reproduce these experimental observations reasonably well [38–41]. In our recent work, an improved AMD with the Fermi motion in the *NN* collision process taken into account explicitly (AMD-FM) [38,42] has been proposed. As demonstrated in Ref. [42], the AMD-FM is capable of simultaneously well reproducing both low- and high-energy proton spectra and angular distributions of ^{40}Ar + ^{51}V at 44 MeV/nucleon measured by Coniglione *et al.* [43], and ^{36}Ar + ^{181}Ta at 94 MeV/nucleon measured by Germain *et al.* [44]. Later, we continued to examine the AMD-FM [45], and found that the experimental LCP energy spectra and angular distributions of ^{12}C + ^{12}C at 95 MeV/nucleon were better reproduced by the AMD-FM calculations incorporating with the statistical decay code Gemini as an afterburner [46], comparing with those from the original AMD+Gemini. As the energy spectra and angular distributions are crucial to the flow determination, the establishment of the AMD-FM provides a favourable opportunity for the study of the abnormal α transverse flow in heavy-ion collisions at intermediate energies.

In this article, we aim to investigate the abnormal α transverse flow behavior in heavy-ion collisions at intermediate energies in the framework of the AMD-FM. In experiments, a measured fragment experiences three processes in general, i.e., dynamical process, sequential decay, and experimental detection, from being generated from the collisions to being measured by detectors. To determine the transverse flow from the dynamics information of the measured fragments, off-line data analyses, i.e., reaction plane reconstruction etc, are also required. In the following, the possible origins which may result in the experimentally observed abnormal α flow mass dependence are examined one-by-one in terms of these aspects. The application of the AMD-FM allows these analyses to be comparable to the real experimental case. This article is organized as follows. In Sec. II, the AMD-FM simulations for this work are briefly introduced. In Sec. III, the possible origins of the experimentally observed abnormal α transverse flow behavior are investigated and discussed in terms of dynamical process, sequential decay, experimental detection and data analysis. In Sec. IV, a summary is given.

II. AMD-FM MODEL SIMULATIONS

AMD-FM is developed on the basis of the AMD of Ono *et al.* [38]. Pauli principle in the AMD-FM are fully respected in an exact manner due to the wave function antisymmetrization of nucleons which is inherited from the AMD. During the nucleon transport, two main processes are involved. One is the mean-field propagation of nucleons governed by a given effective interaction, and the other is the *NN* collision process. In the AMD, the wave packet propagation with time is performed classically by solving the Vlasov equation for the centroids of the wave packets with stochastic two-body collision process. However, in nature, as two nucleons are within the collision distance, the momentum uncertainty increases due to the quantum effect which is also called "Fermi boosting effect."

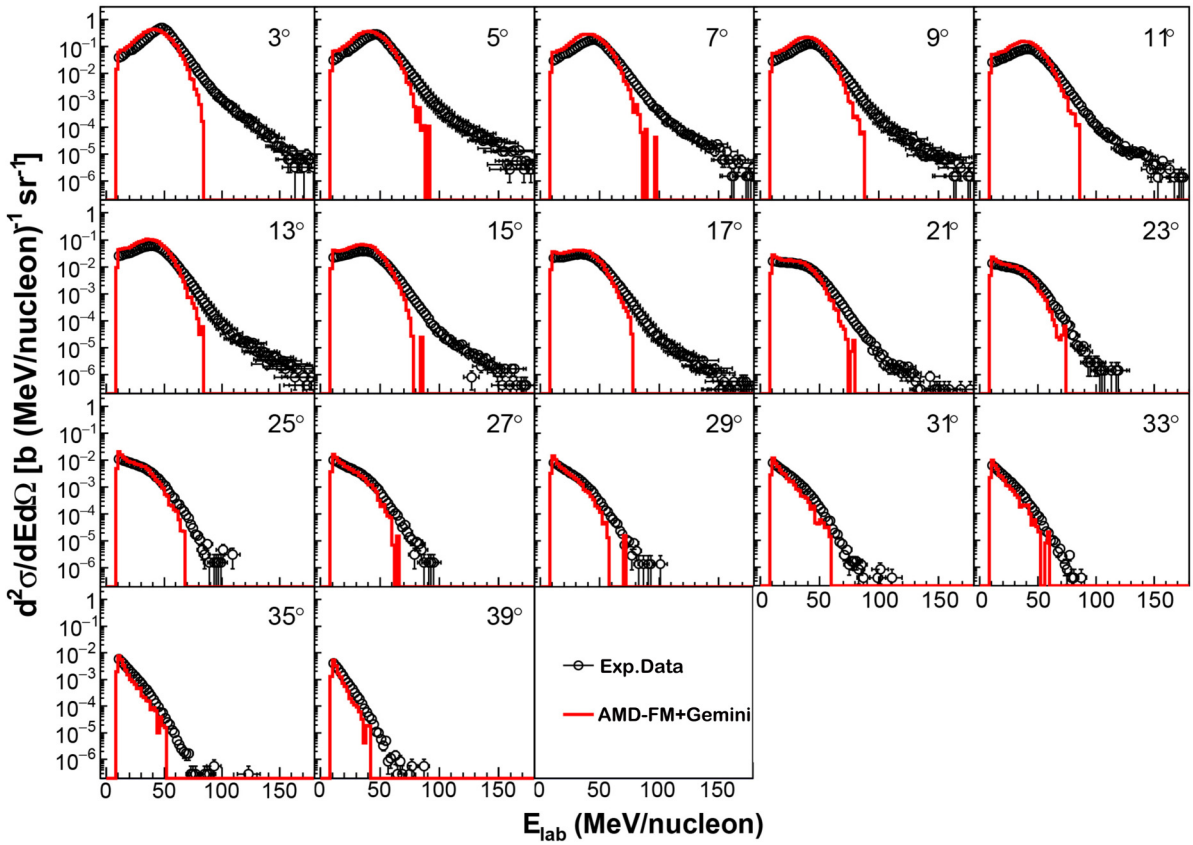

FIG. 2. Comparison between the experimentally measured energy spectra for α particles at entire measured angles from $^{12}C + ^{12}C$ at 50 MeV/nucleon taken from Ref. [48] (circles) and those from the AMD-FM+Gemini simulations (lines).

To take into account the Fermi boosting effect in the NN collisions, the associated momenta $\boldsymbol{P}_1$ and $\boldsymbol{P}_2$ for two given colliding nucleons are written as two parts in the AMD-FM [42],

$$\boldsymbol{P}_i = \boldsymbol{P}_i^0 + \Delta\boldsymbol{P}_i' \quad (i = 1, 2), \tag{1}$$

where $\boldsymbol{P}_i^0$ is the centroid of the Gaussian momentum distribution for the particle i, and the second term, $\Delta\boldsymbol{P}_i'$, is the Fermi momentum randomly given with Gaussian distribution. This treatment is based on the experimental observation of $(e, e'p)$ reactions [47], and different from those in other transport models where the Fermi effect is only taken into account once in the initial nuclei. More detailed description of the AMD-FM can be found in Ref. [42].

Figure 2 presents a typical comparison between the experimentally measured energy spectra for α particles at entire measured angles from $^{12}C + ^{12}C$ at 50 MeV/nucleon taken from Ref. [48], and those from the AMD-FM simulations incorporating with the Gemini (denoted as AMD-FM+Gemini hereinafter). The experimental results are well reproduced by the AMD-FM+Gemini simulations. Same comparisons for protons, deuterons, tritons and ^{3}He are also made, and similar reproduction qualities are obtained. The performance of the AMD-FM is well evidenced by its good descriptions for both energy spectra and angular distributions of LCPs from heavy-ion collisions at intermediate energies, suggesting an advantageous property of the AMD-FM for the present investigation on the abnormal α transverse flow. In this work, 200 000 AMD-FM events of $^{40}Ca + ^{40}Ca$ at 35 MeV/nucleon with fixed impact parameter $b = 4$ fm are simulated using the computer clusters at Cyclotron Institute of Texas A&M University, College Station. For the nucleon transport, the Gogny interaction [49] is taken for the mean field, and the in-medium cross sections of Li and Machleidt [50] is taken for the NN collisions. The nucleon transport process in each event is computed up to 300 fm/c, and primary hot fragments at 300 fm/c are recognized using a coalescence technique with a coalescence radius of 2.5 fm in the coordinate space. Allowing for the sequential decays, the primary hot fragments from the AMD-FM are de-excited using the Gemini code along with our previous work [45].

III. RESULTS AND DISCUSSION

A. Dynamical process

In this work, the microscopic description for dynamical process is simulated by the AMD-FM. The fragments directly from the AMD-FM simulations up to 300 fm/c are analyzed to study the possible origins of the abnormal α flow during the dynamical process. In general, transverse flow are quantified using two equivalent definitions, i.e., slope flow [10,11] and average in-plane transverse momentum flow [51]. For this work, the definition of the slope flow is adopted. For a certain type of fragment with mass number A, the transverse flow is

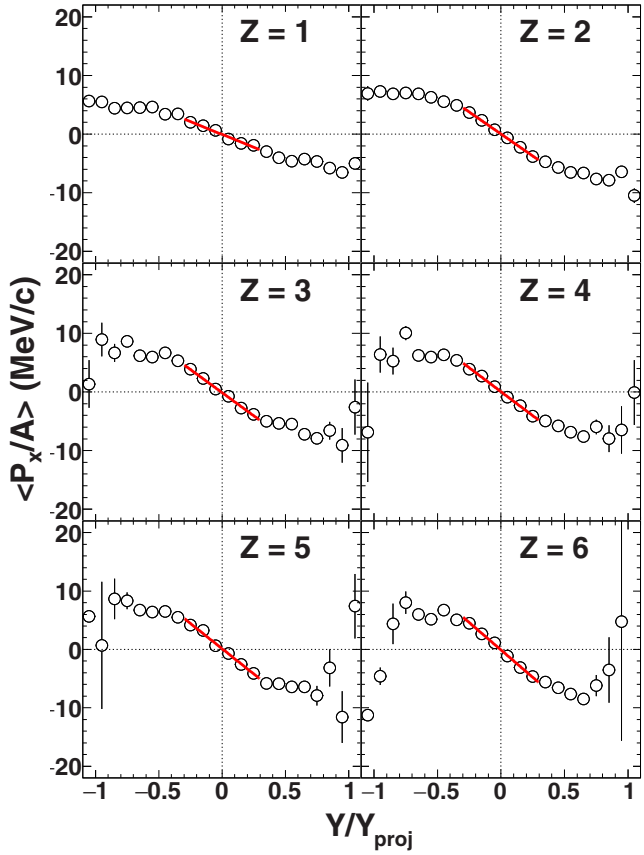

FIG. 3. Average in-plane momentum per nucleon $\langle P_x/A\rangle$ as a function of the scaled rapidity $Y/Y_{\rm proj}$ for $Z = 1$–6 primary fragments from the AMD-FM. Lines depict linear fits for the data in the region of $-0.3 \leqslant Y/Y_{\rm proj} \leqslant 0.3$.

calculated as [10,11]

$$\text{Flow} = \left.\frac{d\langle P_x/A\rangle}{dY}\right|_{Y=0}, \tag{2}$$

where P_x and Y are the in-plane transverse momentum and the rapidity in the center of mass frame, respectively. Y is given by

$$Y = \frac{1}{2}\ln\frac{E + cP_z}{E - cP_z}, \tag{3}$$

where E and P_z are, respectively, the total energy and the longitudinal momentum in the center of mass frame. In practical analysis, the rapidity is often scaled by the center-of-mass rapidity of the projectile [52], so that the projectile (or target) has $Y/Y_{\rm proj} = 1$ (or -1) and the midrapidity region is around $Y/Y_{\rm proj} = 0$. In Fig. 3, the average in-plane momentum per nucleon $\langle P_x/A\rangle$ is plotted as a function of the scaled rapidity $Y/Y_{\rm proj}$ for $Z = 1 - 6$ primary fragments from the AMD-FM events. The solid line in each panel represents the linear fit of data in the region of $-0.3 \leqslant Y/Y_{\rm proj} \leqslant 0.3$. The obtained slope values are plotted by filled circles as a function of Z in Fig. 4, where the error bars are from the linear fit. The negative slopes shown are attributed to the dominance of the attractive mean field at the present incident energy of 35 MeV/nucleon. Note here that the flow as a function of Z, rather than as

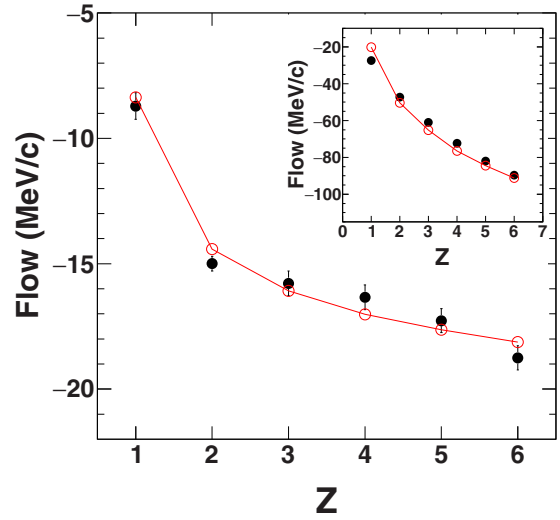

FIG. 4. Flow as a function of Z. Filled circles are the results from the AMD-FM calculations up to 300 fm/c, and open circles are those derived from the CTIM fits. The insert is same but for the results for the CoMD events.

function of A, is used for the present flow mass dependence study, and same hereinafter. This treatment is reasonable, since for the present symmetric system of ^{40}Ca + ^{40}Ca, mass and charge for $Z \geqslant 2$ fragments approximately have a relation of $A = 2Z$. The obtained flow values show a monotonic increase in the negative direction as mass increases, and no abnormal α flow is observed.

To understand this monotonically increasing behavior of the flow with mass from the AMD-FM, a thermodynamic model, collective-thermal-interplay model (CTIM) [32], is applied to elucidate the observed results in Fig. 4. For the present CTIM analysis, fragmentation of a source with mass 80 first takes place using the percolation technique of Staufer *et al.* [53]. The momenta per nucleon of a given fragment with mass number A, P_i/A ($i = x, y, z$, and z direction is the beam direction), are then distributed as a summation of two components, i.e., the thermal component $P_i^{\rm therm}/A$ and the collective component $P_i^{\rm coll}/A$. The thermal component is given by a Maxwellian distribution as

$$f\left(P_i^{\rm therm}/A\right) = \sqrt{\frac{A}{2\pi m_0 T}}\exp\left[-\frac{\left(P_i^{\rm therm}/A\right)^2}{2m_0(T/A)}\right], \tag{4}$$

where T is the temperature of the system at thermal equilibrium and m_0 is the average nucleon mass. For the collective component, only the in-plane transverse flow is taken into account,

$$P_y^{\rm coll}/A = 0, \tag{5}$$

$$P_x^{\rm coll}/A = \tan(\theta_{\rm flow})P_z^{\rm coll}/A, \tag{6}$$

where $\theta_{\rm flow}$ is the flow angle. $P_z^{\rm coll}/A$ is the longitudinal collective momentum per nucleon and it is assumed to obey a

Gaussian distribution such that

$$f\left(P_z^{\rm coll}/A\right) = \frac{1}{\sqrt{2\pi\lambda m_0 T}} \exp\left[-\frac{\left(P_z^{\rm coll}/A\right)^2}{2\lambda m_0 T}\right], \qquad (7)$$

where λ is a free parameter related to the width of the longitudinal collective motion in heavy-ion collisions. From above Eqs. (4)–(7), P_i/A can be sampled by $P_i/A = P_i^{\rm therm}/A + P_i^{\rm coll}/A$, with three parameters, i.e., system temperature T, flow angle $\theta_{\rm flow}$, and λ. Using the temperature value of 5.5 MeV determined from our previous work [54] and taking $\theta_{\rm flow}$ and λ as free parameters, we employ the CTIM to fit the obtained mass dependent flow from the AMD-FM. Permitting to be comparable to the case of heavy-ion collisions, specific consideration for finite system size and momentum conservation is made in the interplay between the thermal motion and the collective motion. In practice, the momentum conservation is carried out by limiting the total momenta $|\sum_j P_i(j)| \leqslant 100$ MeV/c $(i = x, y, z)$ for approximation during the fits. Also since there is no charge information included in the CTIM, the $Z = 1$ flow in Fig. 4 is assumed to be that of $A = 1$ in the CTIM, and those with $Z \geqslant 2$ are assumed to be corresponding to those of CTIM with $A = 2Z$. The fitting results are given by open circles in Fig. 4. As observed in the figure, the monotonically increasing flow trend with mass from the AMD-FM is well reproduced by the CTIM fit (with the parameters of $\theta_{\rm flow} = -15^\circ$ and $\lambda = 0.8$). The good performance of the CTIM suggests a simple dynamical mechanism of the mass-dependent flow in the AMD-FM, that the increasing trend of the flow as fragment mass increases is attributed to the interplay between the thermal motion and the collective motion of fragments from a thermalized fragmenting source.

In actual heavy-ion collisions at intermediate energies, as suggested by the calculations with the quantum molecular dynamics (QMD) model [55], the emissions of LCPs start to occur shortly after the projectile and target make contact, whereas the IMF emissions are with a tendency of coming from cold regions of the system and under a multifragmentation scenario at late stages. This scenario finds support from the experimental observation of Xi *et al.* [56], that temperatures involving carbon isotopes are lower than those with lighter ones. In order to satisfy both the simple mechanism of the interplay between the thermal motion and the collective motion predicted by the CTIM and the emission order difference between LCPs and IMFs simultaneously, the observed monotonically increasing flow trend has to be established at very early stages. Indeed as demonstrated in Fig. 5, the magnitude order of flow with mass are attained at an early period of collisions around 140 fm/c. This fact also explains that the absence of the abnormal α flow in the dynamic process of nuclear collisions, that during the early stages of collisions, α clusters exist in hot nuclear matter and move together with hot nuclear matter, showing no significant difference comparing with nucleons and others. The later global decreasing trend of flows for $Z = 1$–6 fragments with time may be attributed to the final-state interaction [57] and the evaporation of the hot fragments.

It should be mentioned here that this monotonic mass dependence of the flow and its generation mechanism obtained

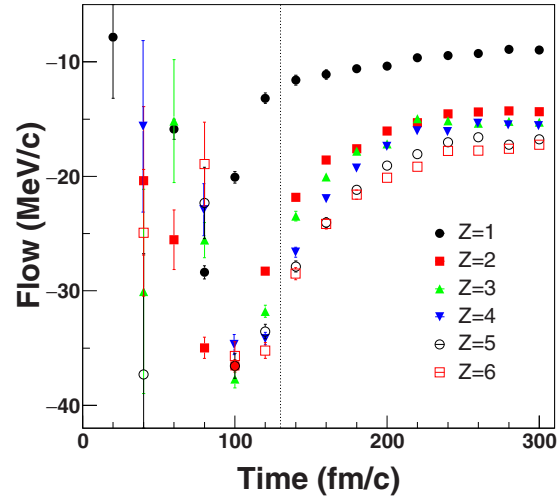

FIG. 5. Time evolution of the flow for $Z = 1$–6 fragments. The flow values for different time are extracted using the linear fits within $-0.3 \leqslant Y/Y_{\rm proj} \leqslant 0.3$.

within the AMD-FM framework are also attained among other QMD-like transport models with different assumptions. To show this, the CoMD simulations [33,34] are performed to generate the events of ^{40}Ca + ^{40}Ca at 35 MeV/nucleon with a fixed impact parameter of 4 fm for comparison. In CoMD calculations, primary fragments are selected at 300 fm/c, and recognized using a coalescence technique with a coalescence radius of 2.5 fm in the coordinate space, for keeping consistency with the case of the AMD-FM. The flow values for $Z = 1$–6 fragments are extracted using the same approach in Fig. 3. The results are plotted in the insert of Fig. 4. It is observed that the CoMD flow shows a monotonically increasing dependence on mass as well, in agreement with that of AMD-FM. The monotonically increasing flow mass dependence is also well reproduced by the CTIM with $\theta_{\rm flow} = -53^\circ$ and $\lambda = 0.4$, demonstrating a similar generation mechanism of mass-dependent flow for the CoMD to that of the AMD-FM. As described in Refs. [33,34], the CoMD is significantly different from the AMD (as well as the AMD-FM for this work), in terms of the effective interaction used for the mean-field propagation of nucleons, the NN collision cross sections, and the treatment of the Pauli principle and in-medium clusterization effect, etc. The AMD-FM and the CoMD are typical among QMD-like transport models. It indicates that the existence of the monotonically mass-dependent flow trend and its dynamical mechanism are independent of these basic modeling assumptions in the AMD-FM and the CoMD, as well as those in other QMD-like transport models. One may also notice that the flow values obtained from the AMD-FM and the CoMD have around five times deviation in magnitude. This can be attributed to the different parameters used in the two models.

B. Sequential decay process

When fragments are formed in intermediate energy heavy-ion collisions, many of them are in excited states and undergo

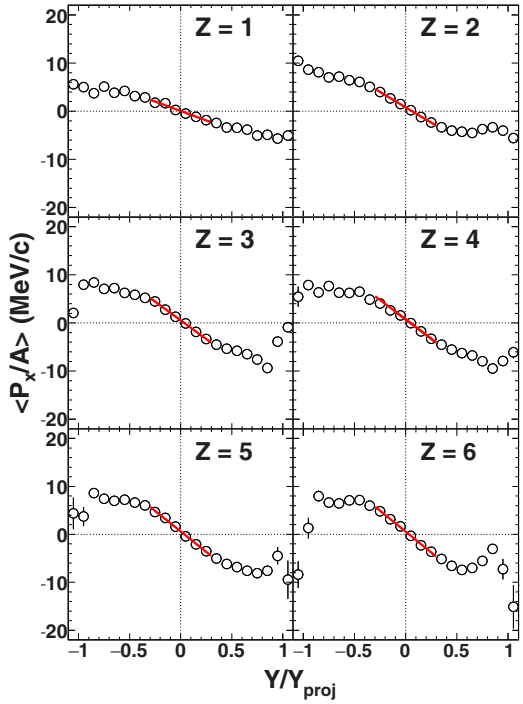

FIG. 6. Same plot as Fig. 3, but for the AMD-FM+Gemini events.

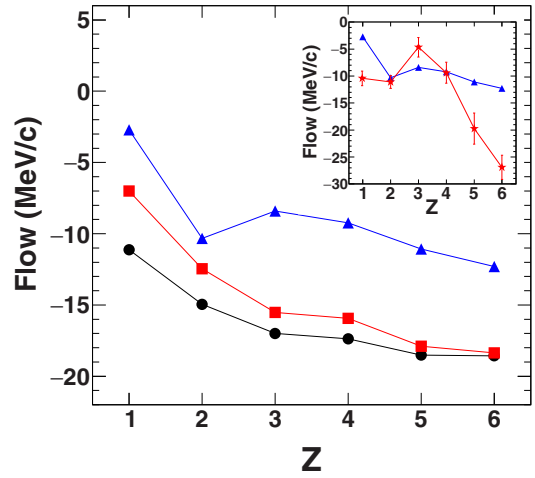

FIG. 7. Same plot as Fig. 4, but for the AMD-FM+Gemini events (circles), for the filtered AMD-FM+Gemini events (squares) and for the filtered AMD-FM+Gemini events where the $\langle P_x/A\rangle$ values are in the reaction planes reconstructed using the AC method (triangles). The insert shows the comparison between the theoretical flow values from the filtered AMD-FM+Gemini events with the reaction planes reconstructed using the AC method (triangles), and the experimental flow values from the events of $^{40}\mathrm{Ca}+^{40}\mathrm{Ca}$ at 35 MeV/nucleon within the impact parameter range of 3-6 fm characterized using the charged particle multiplicity (stars). The experimental results are taken from Ref. [32].

sequential decays prior to being detected in experiments. The dynamical information of the hot and dense nuclear matter during collisions are perturbed by the sequential decays. It may result in serious ambiguities in the flow determination. It is therefore of great necessity to examine whether the abnormal α flow appears after considering the sequential decay process. In Fig. 6, $\langle P_x/A\rangle$ as a function of Y/Y_{proj} for the secondary fragments from the AMD-FM simulations incorporating with the Gemini code as an afterburner is plotted. The extracted flow values from the linear fits within $-0.3 \leqslant Y/Y_{\mathrm{proj}} \leqslant 0.3$ are plotted by circles as a function of Z in Fig. 7. It can be observed that the obtained flow values for the secondary fragments also show monotonically increasing as the fragment mass increases in the overall mass range presented, in rather good agreement with that of the primary fragments. This fact strongly suggests that the experimentally observed abnormal α flow behavior does not originate from the sequential decay process.

C. Experimental detection

Fragments after sequential decays are then measured by detectors in experiments. In this subsection, we continue to investigate the origination of the experimentally observed abnormal α flow behavior, by examining the effects from the experimental conditions using the secondary cold fragments from the AMD-FM+Gemini events. Several detector arrays around the world have been used in the transverse flow studies, i.e., 4π array at Michigan State University [58], Miniball/Miniwall array at Laboratoire National SATURNE [59], INDRA detector array at GANIL [60], NIMROD-ISiS 4π array at Cyclotron Institute, Texas A&M University [61], etc. Here, we refer to one of the most recently established facilities, NIMROD-ISiS 4π array, and examine whether the experimental conditions have an influence on the mass-dependent flow pattern.

NIMROD-ISiS 4π array is a charged particle detector array which consists of 14 concentric rings covering 3.6° to 167° in the laboratory frame. The angular layout of the NIMROD-ISiS array, and the key parameters of detector modules have been given in Table 1 of Ref. [61]. During the experiments, the ejectiles from the collisions first have to hit inside the effective angular range of $3.6^\circ < \theta < 167^\circ$ in order to be detected. Pulse shape discrimination for the fast and slow components of the CsI light output provides isotopic identification of LCPs, and energy loss versus remaining energy in Si-CsI and Si-Si provides isotopic identification for IMFs, in the off-line particle identification (PID) process. This limits that only fragments with kinetic energies large enough to punch through the front Si detector are acceptable for the PIDs. In the present analysis, for keeping consistency with the real case, the secondary cold fragments from AMD-FM+Gemini calculations are filtered first using the angular acceptance of the detector array and the individual front Si wafer punch-through energies of the detector modules. The punch-through energies for various isotopes on 150, 300, and 500 μm Si wafers are calculated using LISE++ [62]. Another experimental condition one should consider carefully is that each detector module itself has a certain angular resolution. Here, for a given fragment, its physical angular information in the laboratory frame directly from AMD-FM+Gemini simulations, θ_{lab} and ϕ_{lab}, are randomized within $\theta_{\mathrm{lab}} \pm \frac{1}{2}\Delta\theta_{\mathrm{det}}$ and $\phi_{\mathrm{lab}} \pm \frac{1}{2}\Delta\phi_{\mathrm{det}}$, where $\Delta\theta_{\mathrm{det}}$ and $\Delta\phi_{\mathrm{det}}$ are the angular

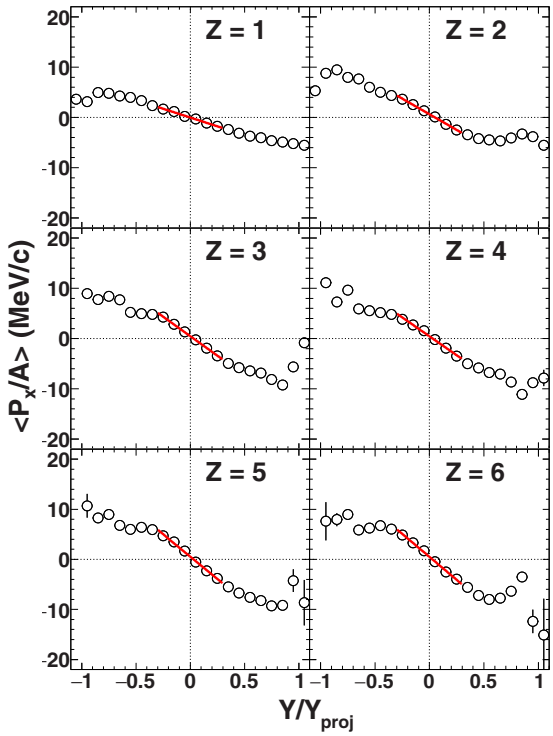

FIG. 8. Same plot as Fig. 3, but for the filtered AMD-FM+Gemini events.

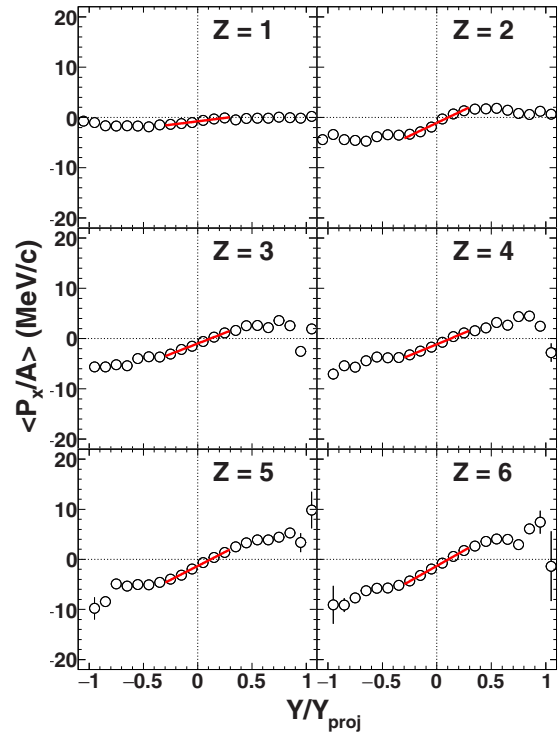

FIG. 9. Same plot as Fig. 3, but for the filtered AMD-FM+Gemini events where the $\langle P_x/A\rangle$ values are in the reaction planes reconstructed using the AC method.

resolutions of the detector module collecting that fragment. Since the NIMROD-ISiS has no capacity of measuring neutron energy and angular information, the neutrons from the simulations are not used for the present analysis. Figure 8 shows the $\langle P_x/A\rangle$ as a function of $Y/Y_{\rm proj}$ for the secondary $Z = 1$–6 fragments filtered by the NIMROD-ISiS filters including the angular coverage of the NIMROD-ISiS array, and the punch-through energies of the front Si detectors (energy thresholds) and the angular resolutions of the detector modules. The extracted flow values are plotted by squares in Fig. 7. The obtained mass-dependent flow shows a monotonically increasing trend, but with reduced magnitudes comparing with those without filtering. These results demonstrate that the flow values are sensitive to the experimental conditions, whereas the experimental conditions do not jeopardize the monotonically mass-dependent flow trend, so that the abnormal α flow does not originate from incomplete experimental fragment detection due to the experimental condition limitations.

D. Data analysis–reaction plane reconstruction

In model simulations, a complete knowledge of in-plane and out-plane momenta for all fragments is available. However, in experiments, one has to reconstruct the reaction plane, which is defined as the plane containing the relative momentum and position vectors of target and projectile nuclei in an event-by-event basis, in prior to determining the in-plane momenta for given fragments. Various methods have been developed for reconstructing reaction planes, i.e., transverse momentum analysis method [63,64], azimuthal correlation method [65], and projectilelike fragment plane method [66], etc. Since the reaction plane reconstruction is rather crucial in the extraction of flow from the experimental data, the contribution from the reaction plane reconstruction process to the mass-dependent flow around α has to be examined carefully. Here, the azimuthal correlation (AC) method is adopted for an example taking the advantage of its good performance at incident energies ranging from the Fermi energy up to around 100 MeV/nucleon [65]. In the AC method, since the transverse momentum is used both for the reaction plane estimation and for the projection, autocorrelations are involved [65]. To avoid the autocorrelation, the particle of interest (POI) is excluded from the estimation of the reaction plane [65]. The reconstructed reaction plane after taking into account the POI effect is also called one plane per particle elsewhere [26].

In Fig. 9, we present the $\langle P_x/A\rangle$ as a function of $Y/Y_{\rm proj}$ for the filtered AMD-FM+Gemini events, where $\langle P_x/A\rangle$ values are evaluated in the reaction planes reconstructed using the AC method. In contrast to Fig. 8, opposite flows are observed here. This is because it is impossible to determine the attractive/repulsive orientation of the reaction plane by the AC method (same for other methods) [65]. This also explains why the experimental flow values are always positive. One may notice the slight offset from the origin in the $\langle P_x/A\rangle$-$Y/Y_{\rm proj}$ plots. Similar nonzero values of $\langle P_x/A\rangle$ at $Y/Y_{\rm proj} = 0$ were also observed in other parallel experiments by Ogilvie *et al.* [64], Pak *et al.* [10], Cussol *et al.* [26], and Kohley *et al.* [13,66]. We have addressed it in our previous work that the origins of the experimentally observed offset are from the asymmetric detection due to the experimental

condition limitations, i.e., the energy threshold and the angular acceptance of the detector array [32]. Since as demonstrated in Figs. 3, 6, and 8 the negative flow is dominant at present incident energy of 35 MeV/nucleon, negative signs are added in front of the extracted slopes to compare with those without the procedure of reaction plane reconstruction. The obtained flow values with negative signs are plotted by triangles in Fig. 7. Of great interest is to observe the appearance of the abnormal α flow behavior. This signal is rather clear and strongly indicates that the abnormal α flow behavior is closely related to the reaction plane reconstruction. The reduced flow values in the overall mass range presented, comparing with those without reaction plane reconstruction, is also a typical indication of the impact induced by the procedures used to reconstruct the reaction plane [26]. In the insert of Fig. 7, the obtained AMD-FM flow values with the reaction plane reconstruction procedure (triangles) are compared with the experimentally extracted flow values from the events of ^{40}Ca + ^{40}Ca at 35 MeV/nucleon from our previous work [32]. One may observe the consistent abnormal α flow enhancement in both experiment and theory, in spite of a significant flow difference in magnitude for both cases. The difference between the experimental and theoretical flow values may be attributed to many factors, i.e., the poor PID in the backward angles in the actual experiment, and the ignored event characterization in the simulations etc. To carry out more quantitative comparison of the flows between the experiments and model simulations, these factors should be carefully considered. For a cross-check, the transverse momentum analysis method is applied to reconstruct the reaction plane, and following the same analysis procedure, similar mass-dependent flow trend to that of Fig. 7 is obtained as well, further confirming the relation between the abnormal α flow behavior and the reaction plane reconstruction.

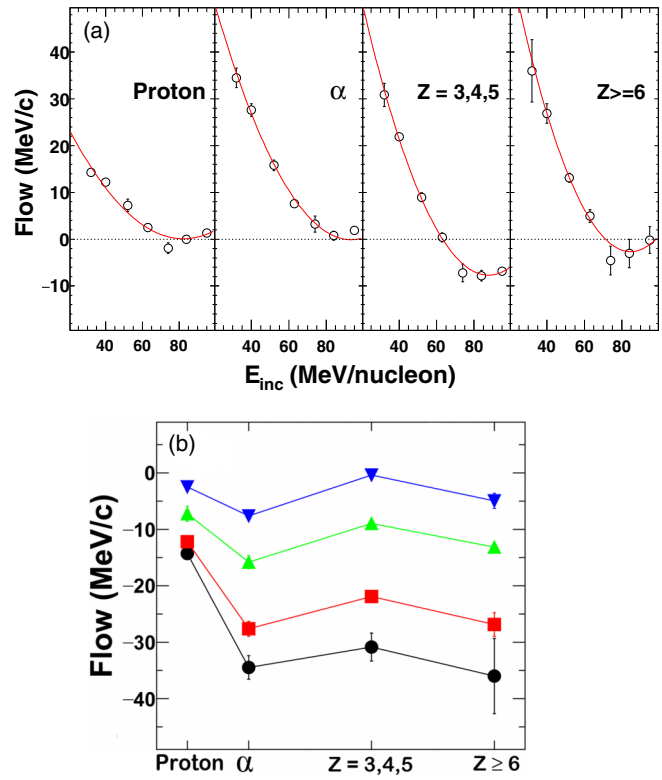

FIG. 10. (a) Flow as a function of incident energy for proton, α, $Z = 3$–5 and $Z \geqslant 6$ fragments from the Ar+Ni system. Circles represent the experimental results directly taken from Ref. [26], and lines are the corresponding quadratic polynomial fittings. (b) Flow as a function of particle type for proton, α, $Z = 3$–5 and $Z \geqslant 6$ fragments at the incident energies of 32, 40, 52, and 63 MeV/nucleon, where the incident energies decrease from top to bottom.

E. Abnormal α flow behavior and reaction plane reconstruction

To understand how the reaction plane reconstruction distorts the monotonically increasing trend of flow with mass and generates the abnormal α flow behavior, we refer to one experimental flow investigation of Cussol *et al.* [26]. In that work, they determined the transverse flow values for the Ar+Ni collisions from 32 to 95 MeV/nucleon and for the Ni+Ni system from 32 to 90 MeV/nucleon to study the balance energies using the GANIL facility with the INDRA detector system [26]. In Fig. 10(a), we show the flow versus incident energy plots for proton, α, $Z = 3$–5, and $Z \geqslant 6$ fragments from the Ar+Ni system by circles for example. The results for deuteron, triton, ^{3}He, which are also available in Ref. [26], and will be discussed later. A typical U shape of flow as a function of incident energy appears for all types of particles. Fitting the data points using quadratic polynomial in each panel, one may get the energy corresponding to the minimum flow value, namely the balance energy. For given type of particles, we take the experimentally determined flow values at the incident energies below the balance energy, 32, 40, 52, and 63 MeV/nucleon, respectively, and plot them as a function of particle type in Fig. 10(b). Due to the symmetry of the U shape of flow as a function of incident energy relative to the balance energy [67], the flow values below the balance energy are taken only. Similar to those by triangles in Fig. 7, negative signs are also added in front of these values. One may observe that the abnormal α flow enhancement exists at all four measured incident energies, and the overall flow mass-dependent patterns are identical to that we obtained in Fig. 7 by triangles.

In Fig. 10(a), it is observed that, in contrast to those of proton and α, the flow versus incident energy plots for $Z = 3$–5 and $Z \geqslant 6$ fragments both show negative flows at incident energies around minima. Similar results are also obtained from the Ni+Ni system [26]. Such results are of great surprise. With a serious examination using models, Cussol *et al.* attributed the negative values around the balance energy to the imperfect performance of the experimental reaction plane reconstruction methods, that reaction plane reconstruction method used to avoid autocorrelations by excluding the POI, leads to an anticorrelation [26]. This anticorrelation only exists in the reaction plane reconstruction of IMFs, and therefore no significant negative flows are observed for proton and α particles in Fig. 10(a). The extracted balance energy of the Ar+Ni system is 82 ± 2 MeV/nucleon, showing no significant dependence on the particle species. It suggests that

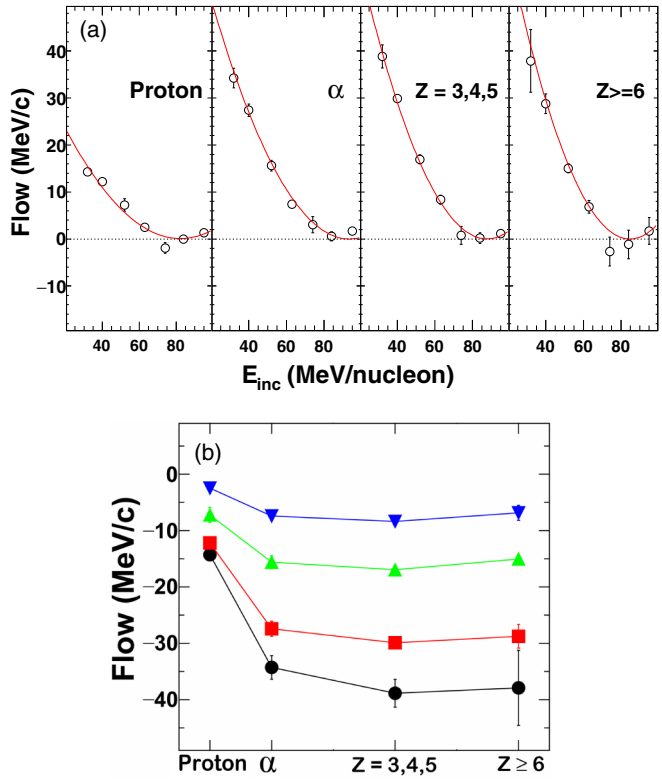

FIG. 11. Same plots as Fig. 10, but for those after the artificial shift in the Y axis to fix the negative offsets around the balance energy.

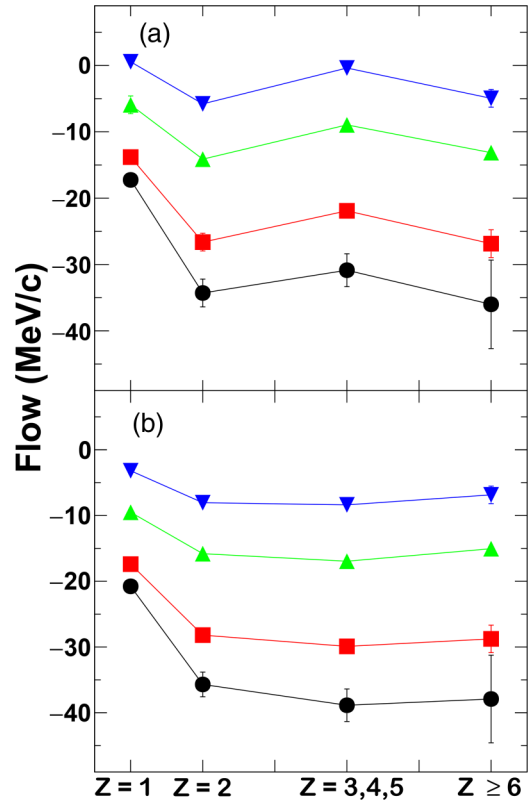

FIG. 12. (a) Same plot as Fig. 10(b), but as a function of Z. (b) Same plot as Fig. 11(b), but as a function of Z. See the details in the text.

although the flow values for the IMFs are negative around the balance energy in Fig. 10(a), the shape of flow as a function of incident energy is still reliable. Following this, one may artificially shift the flow versus incident energy plots of IMFs [shown in Fig. 10(a)] in the Y axis to eliminate the negative flows around the balance energy. The results are given in Fig. 11(a). Using a similar method as that in Fig. 10(b), one can obtain Fig. 11(b). After the artificial shift, it is found in the figure that the abnormality of α flow behavior disappears for all four incident energies, and results in to follow a smoothly increasing mass-dependent trend. Therefore, it can be inferred that the abnormal α flow behavior is artificially generated. That is, the origin of the abnormal α flow behavior is from the flow reduction for IMFs due to the anticorrelation effect from the imperfect performance of the reaction plane reconstruction method. One may also notice a slight reduction of experimental $Z \geqslant 6$ flow in Fig. 11(b). This can be attributed to the system size effect, that at large mass region, the flow decreases with mass originating from the suppression of collective motion due to the momentum conservation [32].

In Ref. [26], the negative flow values around the balance energy have been also found for deuteron, triton and ^{3}He. However, they were attributed to be from the combination of the imperfect reaction plane reconstruction and the dynamics of the collisions, in contrast to those of the IMFs [26]. It is also important to take into account the deuteron, triton, and ^{3}He flows, and examine whether the conclusion above holds consistently. Performing the same artificial flow shift to eliminate the negative flow values around the balance energy, the deuteron, triton and ^{3}He flow values after the artificial flow shift are obtained. To include these flow values, the flow values for $Z = 1$ and $Z = 2$ particles are evaluated to be the average flow values with the weight factors by using the given isotope yields for the given Z. The yields of proton, deuteron, triton, ^{3}He and α emitted in the forward angles from the Ar+Ni collisions with the impact parameter of 0–3 fm (the same range in which the flows were determined by Cussol *et al.* [26]) taken from Ref. [68] for an approximation. When there is no yield information at given energies, the yields are estimated using an interpolation technique. The obtained flow values for $Z = 1$–2 particles before and after the artificial flow shift are plotted as a function of Z together with those for $Z = 3$–5 and $Z \geqslant 6$ particles in Figs. 12(a) and 12(b). The obtained flow trends in the upper and lower panels are in close agreement with those of Figs. 10(a) and 11(b), respectively. The disappearance of the abnormal α flow behavior after the artificial shift demonstrates that the conclusion that the reduction of IMF flows due to the reaction plane reconstruction is the dominant origin of the apparent abnormal α flow enhancement still holds after taking into account the deuteron, triton and ^{3}He flows.

It should be emphasized that the artificial flow shift [from Fig. 10(a) to Fig. 11(a), for example] is rather arbitrary. It can be only treated as a way for explaining the experimentally observed abnormal α flow behavior, rather than an effec-

tive correction of inaccurately determined reaction planes. Based on traditional reaction plane reconstruction methods, as pointed out in Ref. [26], reasonable reaction planes can be achieved only from the complete measurements in experiments, and however, it is an extremely difficult task. Recently, machine-learning techniques have been introduced for particle identification and event characterization in experiment [69,70], making use of its capacity of recognizing and characterizing complex data sets. The perspective of well reconstructing the reaction planes in heavy-ion collisions may also become accessible using the machine-learning techniques in future.

IV. SUMMARY

The experimentally observed abnormal α flow behavior from heavy-ion collisions at intermediate energies is investigated within the framework of an improved AMD with specific consideration of the Fermi motion in the *NN* collision process, AMD-FM. Possible origins of the abnormal α flow in terms of dynamical process, sequential decay, experimental detection and data analysis are examined carefully using the AMD-FM events of $^{40}\mathrm{Ca}+^{40}\mathrm{Ca}$ at 35 MeV/nucleon with a fixed impact parameter of 4 fm. In summary, the conclusions drawn from the present analyses are given as follows:

(i) The flow values determined from the AMD-FM events computed up to 300 fm/c show a monotonically increasing trend as a function of fragment mass, with no exception for the α flow. With the aid of a collective-thermal-interplay model, the increasing trend of the flow with mass is found to originate from the interplay between the thermal motion and the collective motion of fragments from a thermalized nuclear matter. The investigation of the time evolution of the mass-dependent flow demonstrates that the monotonically increasing trend is attained at early stages of collisions. Taking into account of the model dependence effect on the mechanism of the monotonically increasing flow mass dependence, CoMD simulations are performed for comparison. It is found that the flow trend as a function of fragment mass from the CoMD events is in good agreement with that of the AMD-FM. It is suggested that the monotonically mass-dependent flow and its dynamical mechanism are independent of the basic modeling assumptions, i.e., the mean-field propagation of nucleons, the *NN* collisions, the treatment of the Pauli principle and in-medium clusterization effect, etc., between the AMD-FM and the CoMD, as well as those among other QMD-like transport models.

(ii) The examination of whether the abnormal α flow behavior originates from the sequential decay process is performed using the secondary fragments from the the AMD-FM events incorporating with the Gemini code as an afterburner. The flow values for the secondary fragments also increase monotonically with fragment mass, in rather good agreement with that of the primary fragments, demonstrating that the experimentally observed abnormal α flow behavior does not originate from the sequential decay process.

(iii) The experimental filters of the NIMROD-ISiS array, i.e., the angular coverage of the NIMROD-ISiS array, and punch-through energies of the front Si detectors (energy thresholds) and angular resolutions of the detector modules, are applied to the AMD-FM+Gemini events to investigate the effects from incomplete experimental fragment detection due to the experimental condition limitations to the experimentally observed abnormal α flow. It is found that the flow amplitudes are only reduced due to the experimentally filtering, but the monotonically increasing flow trend with mass does not change.

(iv) A key off-line analysis procedure in the flow determination, reaction plane reconstruction, is examined using the filtered events from the AMD-FM+Gemini simulations. The azimuthal correlation method is adopted for example allowing for its good performance in the reconstruction of the reaction planes at intermediate heavy-ion collisions. After introducing the reaction plane reconstruction, the abnormal α flow appears, indicating a close relationship between the abnormal α flow and reaction plane reconstruction. Referring to the flow study of Cussol *et al.* and combining their conclusions [26], it can be inferred that the abnormal α flow is apparent, and the actual origin is mainly from the IMF flow reduction due to the anticorrelation effect originating from the imperfect reconstruction of the reaction planes.

The above conclusions are rather preliminary and within the framework of typical QMD-like transport models only. It will be of great importance to investigate the abnormal α flow using BUU-type transport models in future, i.e., Boltzmann-Uehling-Uhlenbeck model [71], stochastic mean-field model [72], etc., as well as statistical models, i.e., microcanonical metropolitan Monte Carlo model [73] and statistical multifragmentation model [74]. Another remaining open problem is constituted by the inaccurate determination of the reaction planes using the traditional reaction plane reconstruction methods. Applying the machine-leaning techniques may make it possible to increase accuracy of the reaction plane reconstruction.

ACKNOWLEDGMENTS

The authors thank the staff in the Cyclotron Institute, Texas A&M University, for the fruitful conversations. This work is supported by the National Natural Science Foundation of China (Grants No. 11705242, No. U1632138, No. 11805138, and No. 11905120), the Fundamental Research Funds For the Central Universities (Grants No. YJ201954, No. YJ201820, and No. GK201903022) in China, and International Visiting Program for Excellent Young Scholars of Sichuan University.

[1] P. Danielewicz, R. Lacey, and W. G. Lynch, Science **298**, 1592 (2002).
[2] J. M. Lattimer and M. Prakash, Astrophys. J. **550**, 426 (2001).
[3] H. A. Bethe, Rev. Mod. Phys. **62**, 801 (1990).
[4] M. J. Huang, R. C. Lemmon, F. Daffin, W. G. Lynch, C. Schwarz, M. B. Tsang, C. Williams, P. Danielewicz, K. Haglin, W. Bauer, N. Carlin, R. J. Charity *et al.*, Phys. Rev. Lett. **77**, 3739 (1996).
[5] H. H. Gutbrod, A. M. Poskanzer, and H. G. Ritter, Rep. Prog. Phys. **52**, 1267 (1989).
[6] M. D. Partlan, S. Albergo, F. Bieser, F. P. Brady, Z. Caccia, D. Cebra, A. D. Chacon, J. Chance, Y. Choi, S. Costa, J. B. Elliott, M. L. Gilkes *et al.*, Phys. Rev. Lett. **75**, 2100 (1995).
[7] B. Kämpfer, R. Kotte, J. Mösner, W. Neubert, D. Wohlfarth, J. P. Alard, Z. Basrak, N. Bastid, I. M. Belayev, Th. Blaich, A. Buta, R. Čaplar *et al.*, Phys. Rev. C **48**, R955 (1993).
[8] R. Kotte, B. Kämpfer, J. Mösner, W. Neubert, D. Wohlfarth, J. P. Alard, V. Amouroux, Z. Basrak, N. Bastid, I. M. Belayev, L. Berger, Th. Blaich *et al.*, Phys. Rev. C **51**, 2686 (1995).
[9] G. Peilert, H. Stöcker, and W. Greiner, Rep. Prog. Phys. **57**, 533 (1994).
[10] R. Pak, W. Benenson, O. Bjarki, J. A. Brown, S. A. Hannuschke, R. A. Lacey, B.-A. Li, A. Nadasen, E. Norbeck, P. Pogodin, D. E. Russ, M. Steiner *et al.*, Phys. Rev. Lett. **78**, 1022 (1997).
[11] R. Pak, B.-A. Li, W. Benenson, O. Bjarki, J. A. Brown, S. A. Hannuschke, R. A. Lacey, D. J. Magestro, A. Nadasen, E. Norbeck, D. E. Russ, M. Steiner *et al.*, Phys. Rev. Lett. **78**, 1026 (1997).
[12] Z. Kohley, L. W. May, S. Wuenschel, A. Bonasera, K. Hagel, R. Tripathi, R. Wada, G. A. Souliotis, D. V. Shetty, S. Galanopoulos, M. Mehlman, W. B. Smith *et al.*, Phys. Rev. C **82**, 064601 (2010).
[13] Z. Kohley, L. W. May, S. Wuenschel, M. Colonna, M. Di Toro, M. Zielinska-Pfabé, K. Hagel, R. Tripathi, A. Bonasera, G. A. Souliotis, D. V. Shetty, S. Galanopoulos *et al.*, Phys. Rev. C **83**, 044601 (2011).
[14] Z. Kohley, M. Colonna, A. Bonasera, L. W. May, S. Wuenschel, M. Di Toro, S. Galanopoulos, K. Hagel, M. Mehlman, W. B. Smith, G. A. Souliotis, S. N. Soisson *et al.*, Phys. Rev. C **85**, 064605 (2012).
[15] A. Ono and H. Horiuchi, Phys. Rev. C **51**, 299 (1995).
[16] B.-A. Li, Z. Ren, C. M. Ko, and S. J. Yennello, Phys. Rev. Lett. **76**, 4492 (1996).
[17] L. Scalone, M. Colonna and M. Di Toro, Phys. Lett. B **461**, 9 (1999).
[18] L. W. Chen, F. S. Zhang, and Z. Y. Zhu, Phys. Rev. C **61**, 067601 (2000).
[19] B.-A. Li, A. T. Sustich, and B. Zhang, Phys. Rev. C **64**, 054604 (2001).
[20] A. D. Sood and R. K. Puri, Phys. Rev. C **69**, 054612 (2004).
[21] J. Rizzo, M. Colonna, M. Di Toro, and V. Greco, Nucl. Phys. A **732**, 202 (2004).
[22] M. Di Toro, S. J. Yennelloa and B.-A. Li, Eur. Phys. J. A **30**, 153 (2006).
[23] S. Gautam, A. D. Sood, R. K. Puri, and J. Aichelin, Phys. Rev. C **83**, 034606 (2011).
[24] R. Pak, W. J. Llope, D. Craig, E. E. Gualtieri, S. A. Hannuschke, R. A. Lacey, J. Lauret, A. C. Mignerey, D. E. Russ, N. T. B. Stone, A. M. Vander Molen, G. D. Westfall, and J. Yee, Phys. Rev. C **53**, R1469 (1996).
[25] R. Pak, O. Bjarki, S. A. Hannuschke, R. A. Lacey, J. Lauret, W. J. Llope, A. Nadasen, N. T. B. Stone, A. M. Vander Molen, and G. D. Westfall, Phys. Rev. C **54**, 2457 (1996).
[26] D. Cussol, T. Lefort, J. Péter, G. Auger, Ch. O. Bacri, F. Bocage, B. Borderie, R. Bougault, R. Brou, Ph. Buchet, J. L. Charvet, A. Chbihi *et al.*, Phys. Rev. C **65**, 044604 (2002).
[27] J. Xu, L. W. Chen, ManYee Betty Tsang, H. Wolter, Y. X. Zhang, J. Aichelin, M. Colonna, D. Cozma, P. Danielewicz, Z. Q. Feng, A. LeFevre, T. Gaitanos, C. Hartnack, K. Kim, Y. Kim, C. M. Ko, B. A. Li, Q. F. Li, Z. X. Li, P. Napolitani, A. Ono, M. Papa, T. Song, J. Su, J. L. Tian, N. Wang, Y. J. Wang, J. Weil, W. J. Xie, F. S. Zhang, and G. Q. Zhang, Phys. Rev. C **93**, 044609 (2016).
[28] Y. X. Zhang, Y. J. Wang, M. Colonna, P. Danielewicz, A. Ono, M. B. Tsang, H. Wolter, J. Xu, L. W. Chen, D. Cozma, Z. Q. Feng, S. DasGupta, N. Ikeno, C. M. Ko, B. A. Li, Q. F. Li, Z. X. Li, S. Mallik, Y. Nara, T. Ogawa, A. Ohnishi, D. Oliinychenko, M. Papa, H. Petersen, J. Su, T. Song, J. Weil, N. Wang, F. S. Zhang, and Z. Zhang, Phys. Rev. C **97**, 034625 (2018).
[29] J. Xu, Prog. Part. Nucl. Phys. **106**, 312 (2019).
[30] K. G. R. Doss, H. A. Gustafsson, H. Gutbrod, J. W. Harris, B. V. Jacak, K. H. Kampert, B. Kolb, A. M. Poskanzer, H. G. Ritter, H. R. Schmidt, L. Teitelbaum, M. Tincknell *et al.*, Phys. Rev. Lett. **59**, 2720 (1987).
[31] H. Å. Gustafsson, H. H. Gutbrod, J. Harris, B. V. Jacak, K. H. Kampert, B. Kolb, A. M. Poskanzer, H. G. Ritter, and H. R. Schmidt, Mod. Phys. Lett. A **3**, 1323 (1988).
[32] X. Liu, W. Lin, R. Wada, M. Huang, Z. Chen, G. Q. Xiao, S. Zhang, R. Han, M. H. Zhao, P. Ren, Z. Jin, J. Liu, F. Shi, J. B. Natowitz *et al.*, Phys. Rev. C **90**, 014604 (2014).
[33] M. Papa, T. Maruyama, and A. Bonasera, Phys. Rev. C **64**, 024612 (2001).
[34] M. Papa, G. Giuliani, and A. Bonasera, J. Comput. Phys. **208**, 403 (2005).
[35] K. Hagel, M. Gonin, R. Wada, J. B. Natowitz, F. Haddad, Y. Lou, M. Gui, D. Utley, B. Xiao, J. Li *et al.*, Phys. Rev. C **50**, 2017 (1994).
[36] D. Arnett, *Supernovae and Nucleosynthesis* (Princeton University Press, Princeton, NJ, 1996).
[37] X. G. Cao, E. J. Kim, K. Schmidt, K. Hagel, M. Barbui, J. Gauthier, S. Wuenschel, G. Giuliani, M. R. D. Rodriguez, S. Kowalski, H. Zheng, M. Huang *et al.*, Phys. Rev. C **99**, 014606 (2019).
[38] A. Ono and H. Horiuchi, Prog. Part. Nucl. Phys. **53**, 501 (2004).
[39] Y. Kanada-En'yo, M. Kimura, and A. Ono, Prog. Theor. Exp. Phys. **2012**, 01A202 (2012).
[40] R. Wada, K. Hagel, J. Cibor, M. Gonin, Th. Keutgen, M. Murray, J. B. Natowitz, A. Ono, J. C. Steckmeyer, A. Kerambrum, J. C. Angélique *et al.*, Phys. Rev. C **62**, 034601 (2000).
[41] R. Wada, T. Keutgen, K. Hagel, Y. G. Ma, J. Wang, M. Murray, L. Qin, P. Smith, J. B. Natowitz, R. Alfarro, J. Cibor, M. Cinausero *et al.*, Phys. Rev. C **69**, 044610 (2004).
[42] W. Lin, X. Liu, R. Wada, M. Huang, P. Ren, G. Tian, F. Luo, Q. Sun, Z. Chen, G. Q. Xiao, R. Han, F. Shi *et al.*, Phys. Rev. C **94**, 064609 (2016).
[43] R. Coniglione, P. Sapienza, E. Migneco, C. Agodi, R. Alba, G. Bellia, A. Del Zoppo, P. Finocchiaro, K. Loukachine, C. Maiolino, P. Piattelli, and D. Santonocito, Phys. Lett. B **471**, 339 (2000).
[44] M. Germain, P. Eudes, E. Guilbault, P. Lautridou, J. L. Laville, C. Lebrun, M. Leguay, A. Rahmani, T. Reposeur, J. Benlli-

ure, R. Bougault, F. Gulminelli *et al.*, Nucl. Phys. A **620**, 81 (1997).
[45] G. Tian, R. Wada, Z. Chen, R. Han, W. Lin, X. Liu, P. Ren, F. Shi, F. Luo, Q. Sun, L. Song, and G. Q. Xiao, Phys. Rev. C **95**, 044613 (2017), and private communication.
[46] R. J. Charity, M. A. Mcmahan, G. J. Wozniak, R. J. Mcdonald, L. G. Moretto, D. G. Sarantites, L. G. Sobotka, G. Guarino, A. Pantaleo, L. Fiore, A. Gobbi, and K. D. Hildenrand, Nucl. Phys. A **483**, 371 (1988).
[47] I. Bobeldijk, M. Bouwhuis, D. G. Ireland, C. W. de Jager, E. Jans, N. de Jonge, W. J. Kasdorp, J. Konijn, L. Lapikás, J. J. van Leeuwe, R. L. J. van der Meer, G. J. L. Nooren, E. Passchier, M. Schroevers *et al.*, Phys. Rev. Lett. **73**, 2684 (1994).
[48] C. Divay, J. Colin, D. Cussol, Ch. Finck, Y. Karakaya, M. Labalme, M. Rousseau, S. Salvador, and M. Vanstalle, Phys. Rev. C **95**, 044602 (2017).
[49] A. Ono, H. Horiuchi, Toshiki Maruyama, and A. Ohnishi, Prog. Theor. Phys. **87**, 1185 (1992).
[50] G. Q. Li and R. Machleidt, Phys. Rev. C **48**, 1702 (1993); **49**, 566 (1994).
[51] A. Bonasera, F. Gulminelli, and J. Molitoris, Phys. Rep. **243**, 1 (1994).
[52] A. Bonasera and L. P. Csernai, Phys. Rev. Lett. **59**, 630 (1987).
[53] D. Staufer, Phys. Rep. **54**, 1 (1979).
[54] X. Liu, W. Lin, R. Wada, M. Huang, Z. Chen, G. Q. Xiao, S. Zhang, X. Jin, R. Han, J. Liu, F. Shi, H. Zheng, J. B. Natowitz, and A. Bonasera, Phys. Rev. C **90**, 014605 (2014).
[55] C. Schwarz, S. Fritz, R. Bassini, M. Begemann-Blaich, S. J. Gaff-Ejakov, D. Gourio, C. Groß, G. Immé, I. Iori, U. Kleinevoß, G. J. Kunde, W. D. Kunze *et al.*, Nucl. Phys. A **681**, 279c (2001).
[56] H. Xi, W. G. Lynch, M. B. Tsang, W. A. Friedman, and D. Durand, Phys. Rev. C **59**, 1567 (1999).
[57] Q. F. Li, C. Shen, C. Guo, Y. Wang, Z. Li, J. Lukasik, and W. Trautmann, Phys. Rev. C **83**, 044617 (2011).
[58] G. D. Westfall, J. E. Yurkon, J. Van Der Plicht, Z. M. Koenig, B. V. Jacak, R. Fox, G. M. Crawley, M. R. Maier and B. E. Hasselquist, Nucl. Instrum. Methods Phys. Res., Sect. A **238**, 347 (1985).
[59] R. T. de Souza, N. Carlin, Y. D. Kim, J. Ottarson, L. Phair, D. R. Bowman, C. K. Gelbke, W. G. Gong, W. G. Lynch, R. A. Pelak, T. Peterson, G. Poggi *et al.*, Nucl. Instrum. Methods Phys. Res., Sect. A **295**, 109 (1990).
[60] J. Pouthas, B. Borderie, R. Dayras, E. Plagnol, M. F. Rivet, F. Saint-Laurent, J. C. Steckmeyer, G. Auger, C. O. Bacri, S. Barbey, A. Barbier, A. Benkirane *et al.* (INDRA Collaboration), Nucl. Instrum. Methods Phys. Res. A **357**, 418 (1995).
[61] S. Wuenschel, K. Hagel, R. Wada, J. B. Natowitz, S. J. Yennello, Z. Kohley, C. Bottosso, L. W. May, W. B. Smith, D. V. Shetty, B. C. Stein, S. N. Soisson, and G. Prete, Nucl. Instrum. Methods Phys. Res., Sect. A **604**, 578 (2009).
[62] http://lise.nscl.msu.edu.
[63] P. Danielewicz and G. Odyniec, Phys. Lett. B **157**, 146 (1985).
[64] C. A. Ogilvie, D. A. Cebra, J. Clayton, P. Danielewicz, S. Howden, J. Karn, A. Nadasen, A. Vander Molen, G. D. Westfall, W. K. Wilson, and J. S. Winfield, Phys. Rev. C **40**, 2592 (1989).
[65] W. K. Wilson, R. Lacey, C. A. Ogilvie, and G. D. Westfall, Phys. Rev. C **45**, 738 (1992).
[66] Z. Kohley, A. Bonasera, S. Galanopoulos, K. Hagel, L. W. May, A. B. McIntosh, B. C. Stein, G. A. Souliotis, R. Tripathi, S. Wuenschel, and S. J. Yennello, Phys. Rev. C **86**, 044605 (2012).
[67] D. J. Magestro, W. Bauer, O. Bjarki, J. D. Crispin, M. L. Miller, M. B. Tonjes, A. M. Vander Molen, G. D. Westfall, R. Pak, and E. Norbeck, Phys. Rev. C **61**, 021602(R) (2000).
[68] T. Lefort, D. Doré, D. Cussol, Y. G. Ma, J. Péter, R. Dayras, M. Assenard, G. Auger, Ch. O. Bacri, F. Bocage, R. Bougault, R. Brou *et al.*, Nucl. Phys. A **662**, 397 (2000).
[69] P. Baldi, P. Sadowski, and D. Whiteson, Nat. Commun. **5**, 4308 (2014).
[70] G. Kasieczka, T. Plehn, M. Russell, and T. Schell, J. High Energy Phys. 05 (2017) 006.
[71] J. Aichelin and G. Bertsch, Phys. Rev. C **31**, 1730 (1985).
[72] M. Colonna, M. Di Toro, A. Guarnera, S. Maccarone, M. Zielinska-Pfabé, and H. H. Wolter, Nucl. Phys. A **642**, 449 (1998).
[73] D. H. E. Gross, Rep. Prog. Phys. **53**, 605 (1990).
[74] J. P. Bondorf, R. Donangelo, I. N. Mishustin, C. J. Pethick, H. Schulz, and K. Sneppen, Nucl. Phys. A **443**, 321 (1985).